ACS Catalysis

Research Article

pubs.acs.org/acscatalysis

Molybdenum Oxide on Fe_2O_3 Core–Shell Catalysts: Probing the Nature of the Structural Motifs Responsible for Methanol Oxidation Catalysis

C. Brookes,[†,‡] P. P. Wells,*[,†,§] G. Cibin,[⊥] N. Dimitratos,[†,§] W. Jones,[†,‡] D. J. Morgan,[‡] and M. Bowker*[,†,‡]

[†]Rutherford Appleton Laboratory, UK Catalysis Hub, Research Complex at Harwell (RCaH), Harwell, Oxon OX11 0FA, United Kingdom

[‡]Cardiff Catalysis Institute, School of Chemistry, Cardiff University, Main Building, Park Place, Cardiff CF10 3AT, United Kingdom

[§]Department of Chemistry, University College London, 20 Gordon Street, London WC1H 0AJ, United Kingdom

[⊥]Diamond Light Source, Harwell Science and Innovation Campus, Didcot, Oxon OX11 0DE, United Kingdom

Supporting Information

ABSTRACT: A series of MoO_x-modified Fe_2O_3 catalysts have been prepared in an attempt to make core–shell oxidic materials of the type MoO_x/Fe_2O_3. It is conclusively shown that for three monolayers of Mo dosed, the Mo stays in the surface region, even after annealing to high temperature. It is only when the material is annealed above 400 °C that it reacts with the iron oxide. We show by a combination of methods, and especially by XAFS, that at temperatures above 400 °C, most of the Mo converts to $Fe_2(MoO_4)_3$, with Mo in a tetrahedral structure, whereas below that temperature, nanocrystalline MoO_3 is present in the sample; however, the active catalysts have an octahedral MoO_x layer at the surface even after calcination to 600 °C. This surface layer appears to be present at all temperatures between 300 and 600 °C, and it is the nanoparticles of MoO_3 that are present at the lower temperature that react to form ferric molybdate, which underlies this surface layer. It is the MoO_x layer on the $Fe_2(MoO_4)_3$ underlayer that makes the surface active and selective for formaldehyde synthesis, whereas the iron oxide surface itself is a combustor. The material is both activated and improved in selectivity due to the dominance of the methoxy species on the Mo-doped material, as opposed to the much more stable formate, which is the main intermediate on Fe_2O_3.

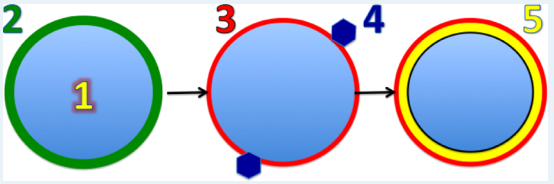

KEYWORDS: *methanol oxidation, formaldehyde synthesis, model catalysts, iron molybdate, XAFS, Raman spectroscopy, core–shell catalysts*

INTRODUCTION

The production of formaldehyde is a very important industrial reaction, with an annual turnover of ∼6 M tons worldwide. Formaldehyde is valued for its ability to act as a unit to higher valued products, including thermosetting resins, adhesives, paper, and fertilizers. Typically, the reaction to formaldehyde involves the oxidative dehydrogenation of methanol, with the first developments of this process recorded in the 1930s. Two main catalytic routes have been identified for this chemistry. First was a silver-catalyzed process,[1,2] which uses a methanol-rich air mixture (at atmospheric pressure) at temperatures between 560 and 600 °C. Formaldehyde yields for this process have been reported to 89%, with the catalyst able to survive for several months. Second, in 1931, Adkin reported the first iron molybdate process.[3] Here, an excess of air is required, with typical reaction temperatures being less than 400 °C. Formaldehyde yield has been reported to be 95%, with the lifetime of these catalysts being 6–12 months.

For the large-scale industrial process, the catalyst typically used is a bulk iron molybdate catalyst with an excess of MoO_3.[4,5] It is thought that the excess MoO_3 primarily acts to replace any molybdenum lost through sublimation at elevated temperatures, which could lead to the formation of the unselective Fe_2O_3 phase. It is a subject of some debate in the literature as to which phase, MoO_3 or $Fe_2(MoO_4)_3$, provides the active site for these reactions. Some consider the $Fe_2(MoO_4)_3$ to be acting solely as the active phase.[6,7] Soares et al. carried out work to rationalize this. Two catalysts, a stoichiometric catalyst (Mo/Fe 1.5:1) and another with Mo excess (Mo/Fe 3:1), were prepared and tested for their ability in the oxidative reaction. They argue that the $Fe_2(MoO_4)_3$ is the active phase because although the increase in the amount of Mo may improve selectivity, the fundamental activity per unit surface demonstrates no change.[8] However, there is a counter argument that MoO_3 is not simply there to replenish any lost molybdena, but is also required for complete selectivity to formaldehyde.[9,10] MoO_3 is highly regarded for its ability to improve the selectivity of this reaction, since an increase in Mo will consequently lead to greater oxygen availability at the

Received: August 14, 2013
Revised: December 4, 2013
Published: December 6, 2013

catalyst surface and changes in activity. Mo-rich catalysts will have a higher capacity to increase surface reoxidation.

House et al. used aberration-corrected scanning transmission electron microscopy(acSTEM), to show that the surface of these catalysts is enriched with Mo.[9] This is also shown by the work of Routray et al. through the use of HRTEM.[11,12] Evidence of Mo segregation has also been supported through reactivity. Fe_2O_3 itself is a highly unselective catalyst for methanol oxidation, with the formate intermediate leading to CO_2 through complete combustion.[6,13] However, with low loadings of Mo, the iron oxide exhibits significantly different selectivity. This suggests that Mo is having a direct effect on the reaction and indicates that the Mo must be predominantly at the surface. Other work from the same group has indicated the active site for the reaction to be Mo (VI), which cycles through Mo (IV) during the reaction.[10] Within this work, several different oxygen sites have been defined and clarified in their roles during this oxidative reaction.

Although the debate regarding the active phase is still ongoing, what is agreed, however, is that the topmost layer of any heterogeneous catalyst is crucial to the efficiency of that material; it is the interface between the catalyst and the reaction phase, so it is important to learn as much as possible about this surface layer. To fully understand the chemistry involved at the surface, it is important to identify not only the phase present but also how this can be related to activity and overall performance of the catalyst.

A broad range of characterization techniques have been used to gain a better understanding of these catalysts. Common techniques for phase identification in these mixed oxides would include Raman,[11,14,15] IR,[16] and XRD.[10,17] Catalytic testing has also been crucial in understanding the chemistry involved. In addition to formaldehyde production, a number of side reactions must also be considered. Although bulk iron molybdates generally possess high selectivity, small amounts of dimethyl ether, dimethoxymethane, methyl formate, and CO are also possible byproducts. Catalysts with excess Mo tend to demonstrate close to 100% selectivity to formaldehyde, with reduced DME byproduct.

A pivotal surface intermediate involved in the reaction is the methoxy, and depending on the surface properties, the methoxy can yield a variety of products.[18] Formaldehyde is seen to be produced over redox sites, DME over acid sites, and CO/CO_2 over basic sites; hence, for bulk MoO_3, the primary product is formaldehyde because the surface of MoO_3 is redox site rich. This eliminates the likelihood for any significant amounts of DME or CO/CO_2. In contrast, Fe_2O_3 is a very poor performer in this reaction. It is shown to be a combustor of methanol, yielding only CO_2 and H_2. This would therefore indicate that a formate intermediate is produced, as shown by Bowker et al.,[6,10,14] as opposed to the methoxy, which is required for selective formaldehyde production.

Although the structures of MoO_3 and $Fe_2(MoO_4)_3$ are reasonably well understood, there still remains some doubt about how they react with methanol, which phase is predominantly involved in the reaction, and especially about the nature of the very topmost surface layers.

The objective of this paper is to determine the nature of the surface layer(s) in the catalysts prepared, in terms of both reactivity and structure, and here we make use of surface layers of Mo oxide (MoO_x) deposited onto an iron oxide powdered catalyst. We denote the samples as MoO_x to differentiate between the MoO_3 phase. Carrying out this method allows us to exclusively analyze surface structural changes by probing changes in Mo structure using XAFS and relate this to changes in catalyst reactivity. XAFS will provide a unique and innovative way of exploring the various structural motifs forming at the surface. XAFS complements other characterization techniques, because it tells us about local geometry, as opposed to long-range structure. A range of other techniques, including electron microscopy, powder XRD, IR, and Raman spectroscopy, have been used here to provide insight into the composition and morphology of these model materials.

RESULTS AND DISCUSSION

To confirm the loading of molybdenum onto the catalyst surface, all samples were analyzed by SEM-EDX mapping. Analysis showed an average Mo loading of 2.7 wt %. TEM-EDX line scans were performed to ensure that catalysts had been prepared homogeneously prior to use in further characterization and testing. Results showed molybdenum to be well dispersed across the iron surface. The images show aggregates of particles in the size range of 30−50 nm. No obvious smaller molybdenum particles were seen to be at the surface of these crystalline iron oxide particles. Ex situ XRD analysis has revealed that for all calcination temperatures, Fe_2O_3 is the only phase detected. There are no separate phases, indicating either that Mo is in an amorphous phase or that we have Mo present in ordered phases of low dimensionality. XPS analysis showed that the Fe and Mo were always in their highest oxidation states of 3^+ and 6^+, and the surface region Mo/Fe declined from an atomic ratio of 0.14 to 0.09 (see the Supporting Information) during annealing from 120 to 600 °C. Finally, BET analysis has been used both before and after catalyst synthesis. The surface area of the bulk MoO_3 sample is very low, with a recorded surface area of 0.7 $m^2\ g^{-1}$. The iron oxide however, has much higher surface area, measuring 21 $m^2\ g^{-1}$. After loading molybdenum onto the iron oxide surface via incipient wetness, there was a small reduction in surface area by 6 $m^2\ g^{-1}$. There were no obvious changes in surface area upon calcination.

Vibrational Spectroscopy. Raman spectra for the bulk phase reference materials and prepared catalysts are shown in Figure 1. The iron oxide shows bands expected for hematite,[19] with major peaks present at 280 and 390 cm^{-1} but that are not shown in Figure 1, which focuses on the Mo-related bands. Molybdena shows significant bands at 820 and 990 cm^{-1} due to

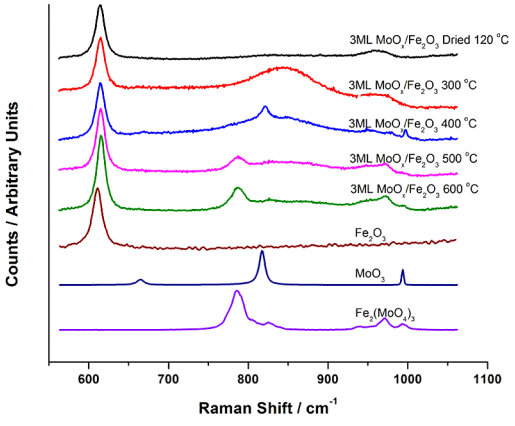

Figure 1. Raman spectra of 3 ML MoO_x/Fe_2O_3, dried at 120 °C and for calcination temperatures of 300, 400, 500, and 600 °C together with reference spectra of Fe_2O_3, MoO_3, and $Fe_2(MoO_4)_3$.

dx.doi.org/10.1021/cs400683e | ACS Catal. 2014, 4, 243−250

Table 1. Raman and IR Vibrational Bands and Their Proposed Assignments for Molybdena and Iron Molybdate Systems

wavenumber (cm^{-1})	band assignment (Raman)	band assignment (IR)
667	symmetric Mo−O−Mo stretch in MoO_3[11,24]	
700−90 broad		tetrahedral species of Mo in $Fe_2(MoO_4)$[25]
780	Mo−O−Mo asymmetric stretch in $Fe_2(MoO_4)_3$[20]	O−Mo−O in $Fe_2(MoO_4)_3$ MoO_4 tetrahedra[25]
817	Mo−O−Mo asymmetric in MoO_3[11]	
850−555		Mo−O−Mo bridge stretch
855−840		v (Fe−Mo−O)
880		Mo−O−Mo stretching[26]
960	terminal Mo═O bond of distorted polymolybdate ions, such as $Mo_7O_{24}^{6-}$ and $Mo_8O_{26}^{4-}$	terminal Mo═O bond of distorted polymolybdate ions, such as $Mo_7O_{24}^{6-}$ and $Mo_8O_{26}^{4-}$
961		Fe−O−Mo vibration[27]
992	terminal Mo═O symmetric stretch in MoO_3[11,15,24]	Mo═O stretching mode in bulk MoO_3

the Mo−O−Mo bridge and Mo═O terminal stretch, respectively (Table 1).[11,20,21] The stoichiometric ferric molybdate sample itself shows similar bands to molybdena, but the main bridging and terminal stretches are shifted to 780 and 960 cm^{-1}. The Raman spectra for the 3 ML MoO_x/Fe_2O_3 catalyst annealed to various temperatures are also detailed in Figure 1, with the spectral range centered around the main Mo-related bands. There is one main band from hematite at 610 cm^{-1}, as expected, because iron oxide is the major material in the sample. However, there are smaller bands due to the presence of Mo in the sample, which are manifested as MoO_3-like features up to 400 °C (990 and 820 cm^{-1}), but after heating above 400 °C, they convert and resemble ferric molybdate (960 and 780 cm^{-1}).

There are, however, some weak remnant molybdena-like peaks. Similar trends are also observed for the infrared spectra (Figure 2) of these materials, with bands detailed in Table 1.[5,22,23] An indicative band for MoO_3 at 990 cm^{-1} is observed for the sample calcined to 400 °C. Bands at a lower wavenumber that we would expect to see for MoO_3 are not present, but this can be explained as a result of the overlap with the other bands present, such as Fe−O−Mo, which is formed through bonding of the Fe_2O_3 to the adsorbed Mo-containing species. Upon calcination to 500 °C, there is a shift of the band at 990 cm^{-1} to 960 cm^{-1}, which is indicative of a phase change to iron molybdate and characteristic of the Fe−O−Mo stretch.

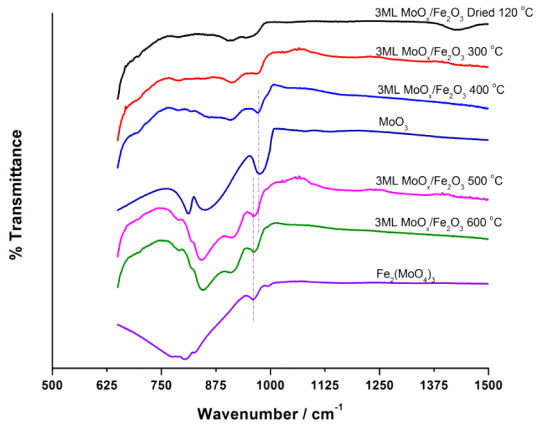

Figure 2. IR spectra of 3 ML MoO_x/Fe_2O_3 dried at 120 °C and after calcination at 300, 400, 500, and 600 °C together with reference spectra of MoO_3 and $Fe_2(MoO_4)_3$.

Electron Microscopy. TEM has proved useful in identifying that the molybdenum is present at the surface of the catalyst. Figure 3 shows a TEM image for a typical particle in a 3 ML MoO_x/Fe_2O_3 catalyst calcined to 500 °C . There are

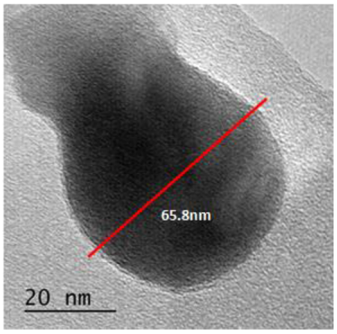

Figure 3. TEM image of a catalyst particle for the 3 ML MoO_x/Fe_2O_3 catalyst, which had been calcined to 500 °C.

no obvious isolated molybdena particles at the surface, indicating that we are more likely to have a layer structure. Particle sizes for the catalyst are typically in the range of 30−50 nm, with results consistent across a range of different areas of the sample in the TEM. Figure 4 shows the accompanying TEM EDX data for the particle in Figure 3. This clearly shows that the outer surface layers are enriched in Mo with a low level of iron compared with the core of the particle. The data evidently show a Mo signal at the edge with a much reduced signal in the core, suggesting that the Mo is concentrated on the surface of the Fe_2O_3 particle. Results were repeated across a range of particles.

XAFS. The XANES spectrum of the dried 3 ML MoO_x/Fe_2O_3 sample (120 °C) compared with those of MoO_3 and $Fe_2(MoO_4)_3$ is shown in Figure 5a. The interpretation of features in the Mo XANES spectra involves the assignment of the pre-edge peak at ∼19 995 eV and the peak at 20 010 eV. The pre-edge peak is attributed to the dipole-forbidden/quadrupole-allowed 1s−4d transition,[28] associated primarily with tetrahedral geometry, but is also present, albeit weaker, in structures with distorted octahedral geometry.[20,29,30] The peak at 20 010 eV is assigned to the dipole-allowed 1s−5p transition and is a characteristic feature of Mo species with octahedral/distorted octahedral geometry.[20,29,30]A comparison of these XANES spectra shows that the dried 3 ML MoO_x/Fe_2O_3 (120 °C) sample has a weaker pre-edge feature than MoO_3, indicating the geometry of Mo is distorted octahedral. The XANES spectrum of MoO_x/Fe_2O_3 (120 °C) is different from MoO_3 in other regions, including a difference in intensity of the peak at 20 010 eV.

dx.doi.org/10.1021/cs400683e | ACS Catal. 2014, 4, 243−250

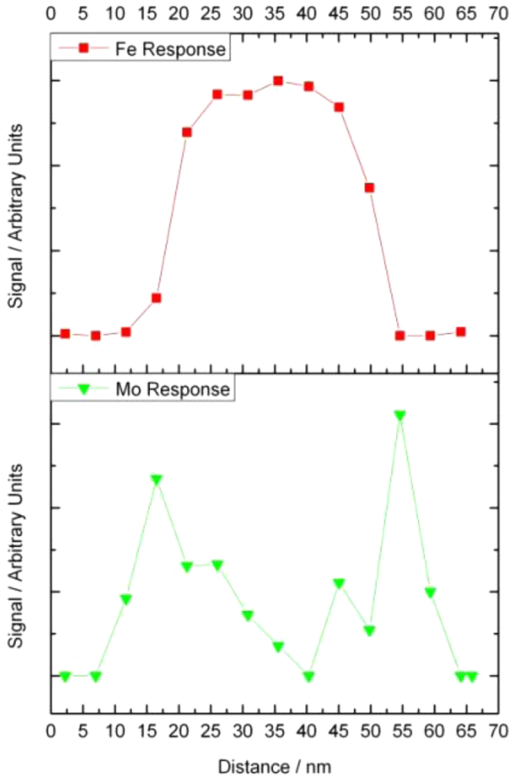

Figure 4. EDX line scan analysis from Figure 3 showing the Fe (top) and Mo (bottom) contributions.

A comparison of the processed XAFS data of MoO_3 and the dried 3 ML MoO_x/Fe_2O_3 (120 °C) sample is shown in Figure 5b. The k^2-weighted χ data show a similar phasing and amplitude for the two samples at values of low k. However, the disparity at higher k suggests that there is less long-range ordering present in the Mo oxide deposited on Fe_2O_3, and fewer high-Z neighbors. This is supported by the radial distribution function (Figure 5c) where the data are dominated by the primary oxygen coordination distances, with only small contributions present at higher values (>3 Å) in R space. This is in contrast to the radial distribution function of MoO_3 where a large secondary shell of Mo neighbors is readily apparent, indicating that the model catalyst Mo has very limited dimensionality.

The effect of the annealing temperature on the nature of Mo within the samples can be seen in the XANES comparison (Figure 5d). By assessing the intensity of the pre-edge peak at 19 995 eV, the XANES spectra show that large amounts of Mo begin to be incorporated into a tetrahedral phase at 500 °C, most likely in the form of $Fe_2(MoO_4)_3$, as indicated by the Raman data, with initial changes in the XANES spectra first seen at 400 °C. No changes are observed in the sample calcined to 300 °C. The k^2-weighted χ spectrum of the 400 °C annealed sample in Figure 5e indicates that the sample is beginning to show features associated with MoO_3 phase formation. An analysis of the phase composition was assessed by performing a linear combination fit of the XANES and χ data (Table 2) using the initial dried sample and MoO_3 as the reference spectra (Figure 5e, f).

The linear combination fits show that a distinct phase of MoO_3 is present in the sample. There is some discrepancy in the relative composition generated by the different linear combination fits, but they both indicate that at these conditions, the MoO_3 phase is being formed. For the samples annealed beyond 400 °C, $Fe_2(MoO_4)_3$ and the dried 3 ML MoO_x/Fe_2O_3 (120 °C) were used as reference spectra for linear combination fit analysis to ascertain the extent of $Fe_2(MoO_4)_3$ formation. Attempts were made to incorporate MoO_3, but more satisfactory fitting parameters were determined without the inclusion of this reference spectrum.

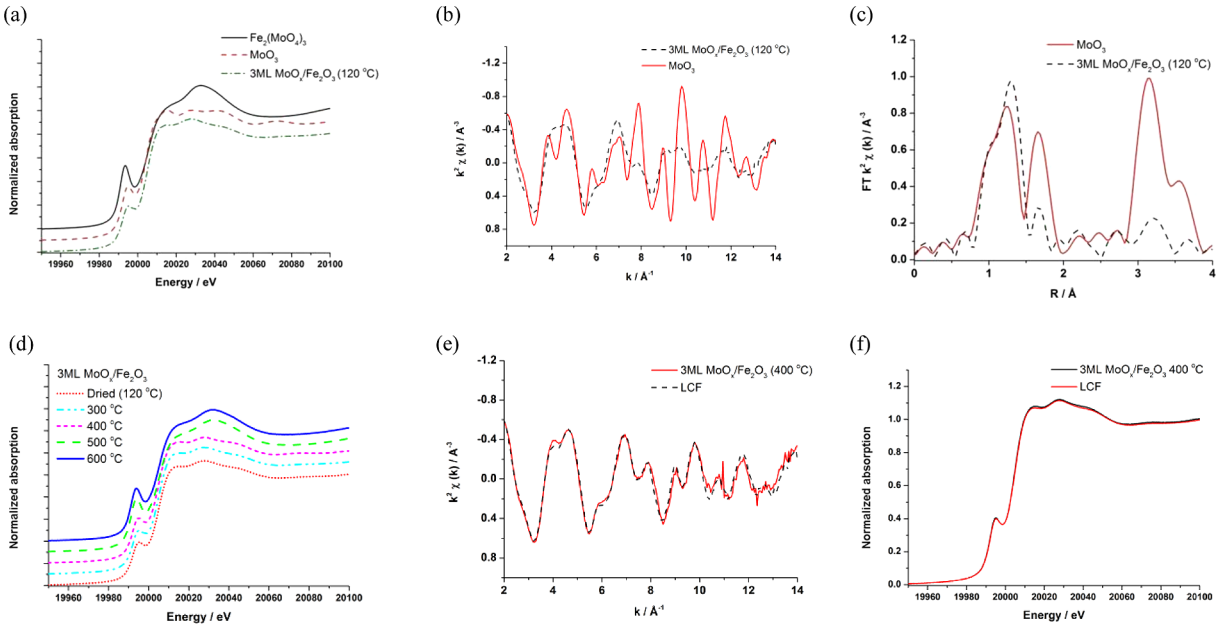

Figure 5. (a) Normalized XANES spectra of dried 3 ML MoO_x/Fe_2O_3 (120 °C), MoO_3, and $Fe_2(MoO_4)_3$; (b) k^2-weighted experimental data and (c) Fourier transform for 3 ML MoO_x/Fe_2O_3 (120 °C) and MoO_3; (d) XANES spectra of 3 ML MoO_3/Fe_2O_3 catalysts annealed to different temperatures and linear combination fits (LCF) of 3 ML MoO_x/Fe_2O_3 (400 °C) using MoO_3 and 3 ML MoO_x/Fe_2O_3 (120 °C) as standards fitted in (e) χ and (f) normalized XANES.

dx.doi.org/10.1021/cs400683e | ACS Catal. 2014, 4, 243−250

Table 2. XANES Linear Combination Fit (LCF) Analysis[31]

sample	reference standards (%)			
	MoO_3	MoO_x/Fe_2O_3	$Fe_2(MoO_4)_3$	R_{factor}
3 ML MoO_x/Fe_2O_3 (300 °C) XANES fit	0	100		0
3 ML MoO_x/Fe_2O_3 (400 °C) XANES fit	14	86		7×10^{-5}
3 ML MoO_x/Fe_2O_3 (400 °C) chi fit	25	75		0.03
3 ML MoO_x/Fe_2O_3 (500 °C) XANES fit		32	68	1×10^{-4}
3 ML MoO_x/Fe_2O_3 (600 °C) XANES fit		34	66	2×10^{-5}

The XANES spectra with associated linear combination fits can be seen in Figure 6, with tabulated values of the phase

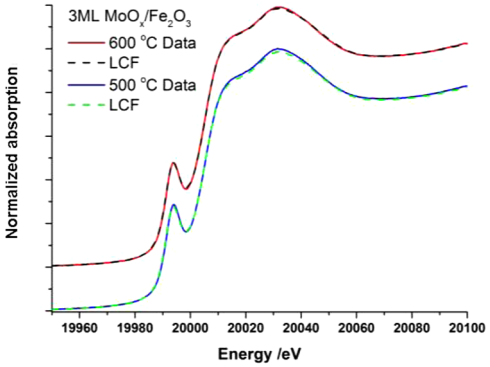

Figure 6. XANES linear combination fits of (a) 3 ML MoO_x/Fe_2O_3 500 °C and (b) 600 °C using $Fe_2(MoO_4)_3$ and 3 ML MoO_x/Fe_2O_3 (120 °C) as standards.

composition shown in Table 2. The data generated from the linear combination fits show that the spectra can be modeled to a large degree of confidence using these reference spectra.

The data confirm that significant amounts of the tetrahedral $Fe_2(MoO_4)_3$ phase is formed at ~500 °C; however, it can also been seen that a large amount (34%) of the MoO_x phase, similar in nature to the dried catalysts, remains, even after annealing at 600 °C. The results show that the amorphous Mo oxide is converted into two forms with annealing. A single layer is left in the surface region, which covers the whole sample (see reactivity data below), but it is also converted into a more crystalline MoO_3 at ~400 °C. Upon annealing above this temperature, the monolayer form remains, but the loss of crystalline MoO_3 from the Raman and XANES spectra is coupled with the formation of $Fe_2(MoO_4)_3$.

Reactivity. We have examined the reactivity of the 3 ML samples for the oxidation of methanol by using reaction measurements and TPD (temperature programmed desorption), and have compared them with the reactivity of standard samples of Fe_2O_3, MoO_3, and $Fe_2(MoO_4)_3$. Figure 7 shows the TPD for the iron oxide, which yields predominantly CO_2 (*m*/*e* 44), hydrogen (*m*/*e* 2), and water (*m*/*e* 18) in a peak at ~290 °C, which is likely to be the result of formate decomposition,[6,10,32] together with a small amount of desorption of methanol (*m*/*e* 31) at ~100 °C. Molybdenum oxide and iron molybdate give only formaldehyde (*m*/*e* 30), with a peak at around 180 °C, due to methoxy decomposition,[6,10] and the

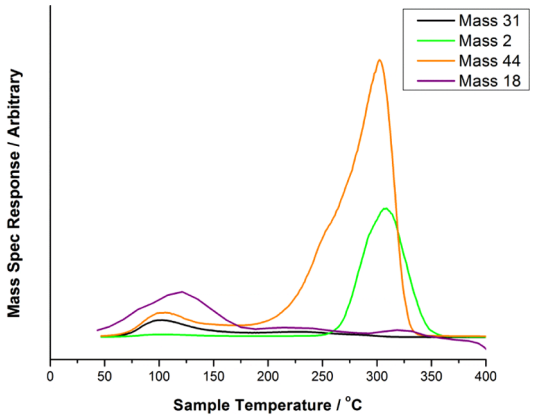

Figure 7. TPD for Fe_2O_3 demonstrating that the dominant products are hydrogen (*m*/*e* 2) and carbon dioxide (*m*/*e* 44), water (*m*/*e* 18), and methoxy (*m*/*e* 31 are also present).

TPD are similar for the two; hence, the TPD for iron molybdate only is shown in Figure 8.

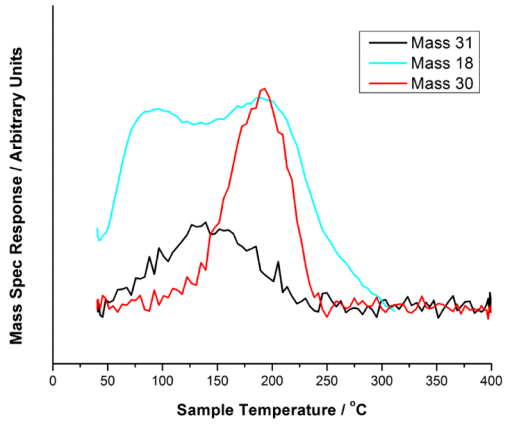

Figure 8. TPD data for bulk $Fe_2(MoO_4)_3$. Here, the dominant products are formaldehyde (*m*/*e* 30) and water (*m*/*e* 18).

The TPD from the 3 ML MoO_x/Fe_2O_3 sample yields mainly formaldehyde with the absence of any CO_2 production (Figure 9). This is a key indicator that the surface comprises no

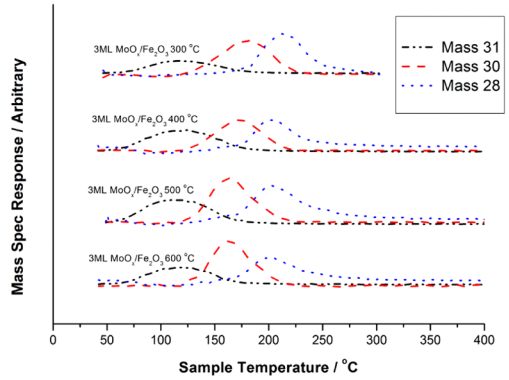

Figure 9. TPD data for 3 ML MoO_x/Fe_2O_3 catalysts calcined to 300, 400, 500, and 600 °C. Note that the contributions the 28 signal from methanol (*m*/*e* 31, peaking at ~120 °C) and formaldehyde (*m*/*e* 30, peaking at ~170 °C) have been removed, leaving only that from CO itself at ~200 °C (*m*/*e* 28).

dx.doi.org/10.1021/cs400683e | ACS Catal. 2014, 4, 243−250

extended iron oxide, that the surface has been significantly modified, and that it is largely composed of Mo species. There is a difference from Mo alone, however, and from iron molybdate because there is a significant amount of CO desorbed (m/e 28), which indicates a mixed layer with both Fe and Mo present. This assignment has been described before for catalysts in which the bulk ratio of Fe and Mo has been varied;[14] however, there is evidence that there is some change in the reactivity pattern with annealing temperature, with the intensity of CO desorption diminishing relative to formaldehyde at increased annealing temperatures (clearly seen in the peaks at ~170 °C from formaldehyde and at ~200 °C from CO). Table 3 shows the selectivities for formaldehyde

Table 3. Data Derived from TPD Experiments

	peak temp, °C		
anneal temp, °C	H_2CO peak	CO peak	selectivity to H_2CO
300	180	210	77
400	170	200	79
500	162	200	82
600	162	197	85

determined from the TPD data, together with the peak temperatures. Note that Figure 9 shows the raw signals, whereas the selectivities are calculated by taking into account the different cracking patterns of formaldehyde and CO, which contribute to the total integral. Because the only products seen in TPD are formaldehyde and CO, selectivity is calculated as $H_2CO/(H_2CO + CO)$. It is clear that shifts in the peak temperatures occur, especially noticeable after annealing at 500 and 600 °C. The formaldehyde peak appears to shift slightly lower in temperature, from 180 to 162 °C, and the CO peak moves from 210 to 200 °C. Table 3 shows the selectivity of the two products for different annealing conditions, although we must remember that this is a transient experiment, so selectivity has a meaning somewhat different from that for the usual steady state experiments.

Notwithstanding these peak shifts, there is little apparent difference in activity of these samples, all giving 50% conversion by ~175 °C (Figure 10) and with significant changes in the overall selectivity to formaldehyde only occurring at high

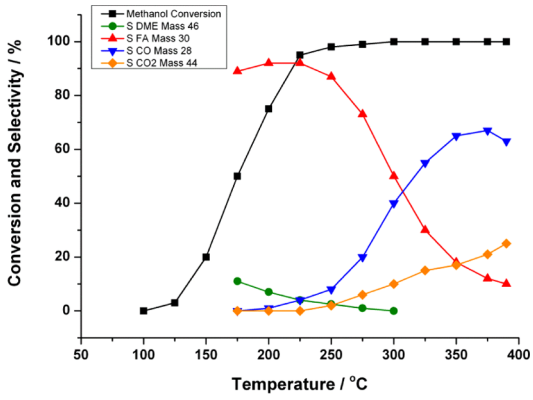

Figure 10. Methanol oxidation reaction measurements over the 3 ML sample annealed to 500 °C, showing the conversion of methanol and the selectivity to the various products observed. Note that there is little change in this profile for different anneal temperatures between 300 and 600 °C, but see Table 4.

conversion (Table 4). The 300 °C sample has a lower selectivity to formaldehyde at high temperatures, and produces

Table 4. The Effect of Annealing on the Selectivity of the 3 ML MoO_x/Fe_2O_3 Catalysts

	selectivity to H_2CO at		
anneal temp, °C	conversion 50%; T = 175 °C	conversion 90%; T = 225 °C	conversion ~100%; T = 300 °C
300	85	80	10
500	89	92	50

much more CO, in line with the effects in the TPD. If we make comparison with the earlier data we obtained for bulk loading variations of Mo in the iron oxide, it is apparent that these data are between the results for bulk ratios of 1:1 and 1:1.5 Fe/Mo.[14] These 3 ML samples also behave much better than those for 6 ML reported in a recent publication,[32] in which the maximum yield was ~55%. Here, the maximum yield is ~85% at about 225 °C, which is similar to high bulk loading catalysts, although the selectivity at high temperature is a lot lower with much more CO production. The main differences from the materials reported here are that the 6 ML samples were (i) calcined in situ in 10% O_2/He and (ii) calcined for only 40 min at 400 °C. Here, calcination was done in air for 2 h. As Huang et al. have shown, "spreading" of the MoO_3 phase over such catalysts appears to be a relatively slow process and requires temperatures over 400 °C for several hours.[33]

The XAFS generally supports the reactivity pattern described above, showing that tetrahedral Mo, in the form of $Fe_2(MoO_4)_3$ is formed on a catalyst calcined to ~500 °C. This is also supported by the Raman and infrared studies; however, it must be noted that not all the Mo is incorporated into the $Fe_2(MoO_4)_3$ phase. Similar observations for reactivity were made when making bulk catalysts with varying bulk loadings of Mo.[14] Even at very low bulk loadings, the combustion capability of Fe_2O_3 was quickly eliminated;. however, in the intermediate range of Mo loading less than 1:5 Mo/Fe ratio, CO is seen as a major product in reactivity studies. This was proposed to be due to the presence of isolated Fe sites at the surface.[14] The reactivity and TPD seen here is similar to that for a bulk ratio of >1:1 Mo/Fe ratio and <1.5 and further implies that some Fe sites are present at the surface. However, there is also significant Mo present there, and both the XAFS and the remnant 980 and 820 cm^{-1} bands in Raman indicate the presence of octahedral Mo sites, which we propose to be at the surface. Indeed, we also have shown that the fully selective catalysts consist of a complete layer of molybdenum oxide at the surface of ferric molybdate.[10,32]

As a result of all these measurements, we propose that the evolution of surface structure is as shown in Figure 11. After calcination at 300 °C, we have a surface that appears to contain a layer of very well dispersed, amorphous Mo oxide on the iron oxide, showing broad peaks in Raman and local coordination. However, heating to 400 °C produces sharper bands in the Raman, clearly as a result of the presence of crystalline MoO_3, and XAFS shows the presence of octahedral Mo, and it is likely that these exist in the form of very small MoO_3 nanoparticles; however, we failed to identify these in TEM, but they could be very few in number relative to the iron oxide particles. Further annealing to 500 °C reduces the amount of MoO_3 forming ferric molybdate, and this is confirmed by XAFS, which has a significantly reduced octahedral component. However, as

dx.doi.org/10.1021/cs400683e | ACS Catal. 2014, 4, 243−250

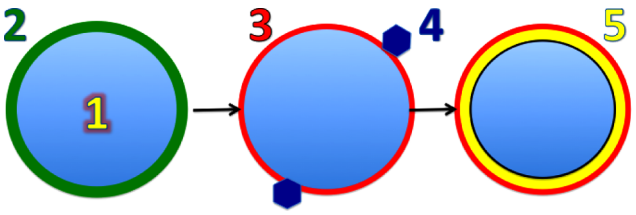

Figure 11. The evolution of the surface structure of the 3 ML catalyst as a function of annealing. On the left, the surface consists of an amorphous MoO_x layer (2), supported on the Fe_2O_3 core (1), which is the structure at low temperatures. In the middle, we show the structure at ~400 °C with both nanocrystallites of MoO_3 (4) at the surface of the catalysts and the surface of MoO_x present. Finally, in the right-hand panel, we have the structure after annealing, in which the nanoparticles of MoO_3 have mostly converted to ferric molybdate (yellow layer 5), but with the active monolayer overlaying it.

described above, the reactivity does not change so much with these structural changes, and we believe that this is because of the presence of a third, crucially important component of the surface structure, which is, in fact, the dominant surface component. This is the surface layer of a Mo-containing material, which we propose is formed already by 300 °C and is the main selective site for formaldehyde production. The extra MoO_3 crystallites, which are present at 400 °C, essentially react with Fe_2O_3 when heated to 500 °C to make underlayers of ferric molybdate, which are at the surface of the iron oxide but which underlie the topmost surface layer. This topmost layer is composed of some Fe with the Mo because we see CO in the TPD, whereas pure Mo surfaces yield only formaldehyde.

CONCLUSIONS

We have investigated the reactivity of a thin layer of Mo on Fe_2O_3 and have found that

(i) The Mo stays in the surface layers even after annealing to 600 °C.
(ii) The Mo forms several phases, depending on annealing temperature: namely, a MoO_x layer with short-range order only; a crystalline form of MoO_3; and subsurface ferric molybdate, which is formed from the latter after annealing above 400 °C.
(iii) Notwithstanding these changes, the reactivity of the surface is largely unchanged by annealing between 300 and 600 °C, showing that the MoO_x layer covers most of the surface over the whole temperature range.
(iv) The conversion and selectivity of this material are close to those of bulk iron molybdate catalysts, again confirming that the active surface is a MoO_3-like layer. It is less selective because of the exposure of some Fe sites at the surface.

EXPERIMENTAL SECTION

Synthesis. A series of catalysts were prepared of MoO_x/Fe_2O_3 by doping 3 ML equiv of Mo oxide onto the surface of commercial Fe_2O_3 (Sigma Aldrich, <50 nm particle size). Fe_2O_3 was first calcined at 500 °C for 3 h in preparation for its use as a support. The desired amount of aqueous ammonium heptamolybdate for 3 ML MoO_x/Fe_2O_3 was dosed onto the surface of the Fe_2O_3 by incipient wetness impregnation with constant mixing. The samples were dried at 120 °C for 24 h before being subjected to different annealing temperatures in air for 2 h.

Bulk phase reference samples were synthesized for comparison with the 3 ML dosed materials. The bulk iron molybdate catalyst with a Mo/Fe ratio of 1.5:1 was prepared using a conventional coprecipitation method. For the preparation, a solution of iron nitrate nonahydrate (Sigma Aldrich, >98%) was added dropwise to a stirring solution of ammonium heptamolybdate (Fluka Analytical, >99%) previously acidified to pH 2 with dilute HNO_3. The resulting mixture was heated to 90 °C for ~1 h until a yellow sludge remained. This was left to air-dry overnight, after which it was dried at 120 °C for 24 h, followed by calcination at 500 °C for 48 h.

Catalytic Testing. Reactor data were obtained by use of a CATLAB reactor (Hiden Ltd., Warrington U.K.). For the catalytic reaction, 1 μL of liquid methanol was injected every 2 min into a flow of 10% O_2/He, at a flow rate of 30 mL min^{-1}. The products were determined by the online mass spectrometer in the CATLAB system. Data such as those in Figure 10 were obtained by applying a temperature ramp to the reactor of 12 °C min^{-1} during the measurements to derive the temperature profile of the reactivity. The results of such pulsed flow experiments are similar to those for steady state experiments carried out in the same reactor in terms of selectivity/conversion vs temperature profiles. For the TPD, ~6 injections of 1 μL methanol were dosed onto the catalyst at ambient temperature in a flow of 30 mL min^{-1} of He. This was followed by ramping the temperature to 400 °C at a rate of 8 °C min^{-1} while monitoring the products formed by mass spectrometry.

Characterization. BET measurements were taken for the commercial Fe_2O_3 (~21 m^2 g^{-1}) and 3 ML catalysts (~15 m^2 g^{-1}). The BET surface area was measured three times for each sample under nitrogen physisorption at 77 K using a Micromeretics Gemini surface area analyzer. Determination of phase composition of the prepared catalysts utilized a range of techniques, including vibrational spectroscopy. Raman measurements were carried out using a Renishaw Raman microscope with an 830 nm laser power over a wavenumber range of 100–1200 cm^{-1}. Typical measurements used a 0.1% laser power, with four accumulations at 10 s exposure time for each. XRD was performed on a Panalytical X'pert pro analyzer with Cu Kα radiation. The IR data were recorded using a Thermo Scientific Nicolet iS10 FT-IR spectrometer using an ATR accessory in the range of 500–2500 cm^{-1}.

Catalyst morphology and homogeneity were examined by both TEM and SEM. TEM was used to ensure samples were prepared homogeneously. The catalysts were examined using a JEOL JEM 2100 EM model and showed no obvious sign of particle clustering or agglomeration at the surface. SEM EDX analysis was carried out using a JEOL JSM- 6610LV model.

Mo k-edge XAFS studies were carried out on the B18 beamline at the Diamond Light Source, Didcot, U.K. Measurements were performed using a QEXAFS setup with a fast-scanning Si(111) double crystal monochromator. The time resolution of the spectra reported herein was 5 min/spectrum (k_{max} = 18). On average, three scans were acquired to improve the signal-to-noise level of the data. All samples were diluted with cellulose and pressed into pellets to optimize the effective edge-step of the XAFS data and measured in transmission mode using ion chamber detectors. All transmission XAFS spectra were acquired concurrently with a Mo foil placed between I_t and I_{ref}.

dx.doi.org/10.1021/cs400683e | ACS Catal. 2014, 4, 243–250

XAS data processing and EXAFS analysis were performed using IFEFFIT[34] with the Horae package[31] (Athena and Artemis). The amplitude reduction factor, s_0^2, was derived from EXAFS data analysis of the known Mo reference compound, MoO_3 (with known coordination numbers, which were fixed during analysis), to be 0.82, which was used as a fixed input parameter.

■ ASSOCIATED CONTENT

Supporting Information

Additional information as noted in text. This material is available free of charge via the Internet at http://pubs.acs.org.

■ AUTHOR INFORMATION

Corresponding Authors

*E-mail: bowkerm@cardiff.ac.uk.

*E-mail: peter.wells@rc-harwell.ac.uk.

Notes

The authors declare no competing financial interest.

■ ACKNOWLEDGMENTS

We thank the EPSRC for supporting the activities of the UK Catalysis Hub at RCaH and the grant for funding Dr. P. P. Wells (Catalytic Science in the Harwell Research Centre EP/I019693/1). Thanks also go to Diamond Light Source and the Cardiff Catalysis Institute (CCI) for funding the studentship of Catherine Brookes. The authors thank Diamond Light Source for the allocation of beamtime (SP8071-1) and support of their staff. We also thank RCaH and their staff, especially Iain Walmsley, for all the support provided.

■ REFERENCES

(1) Cao, Y.; Dai, W. L.; Deng, J. F. *Appl. Catal., A* **1997**, *158*, L27−L34.

(2) Qian, M.; Liauw, M. A.; Emig, G. *Appl. Catal., A* **2003**, *238*, 211−222.

(3) Adkin, H.; Peterson, W. R. *J. Am. Chem. Soc.* **1931**, *53*, 1512.

(4) Soares, A. P. V.; Portela, M. F. *Catal. Rev. Sci. Eng.* **2005**, *47*, 125−174.

(5) Soares, A. P. V.; Portela, M. F.; Kiennemann, A.; Hilaire, L.; Millet, J. M. M. *Appl. Catal., A* **2001**, *206*, 221−229.

(6) Bowker, M.; Holroyd, R.; Elliott, A.; Morrall, P.; Alouche, A.; Entwistle, C.; Toerncrona, A. *Catal. Lett.* **2002**, *83*, 165−176.

(7) Abaulina, L. I.; Kustova, G. N.; Klevtsova, R. F.; Popov, B. I.; Bibin, V. N.; Melekhina, V. A.; Kolomiichuk, V. N.; Boreskov, G. K. *Kinet. Catal.* **1976**, *17*, 1126−1132.

(8) Sunkou, M. R.; Mendioroz, S.; Fierro, J. L. G.; Palacios, J. M.; Guerreroruiz, A. *J. Mater. Sci.* **1995**, *30*, 496−503.

(9) House, M. P.; Shannon, M. D.; Bowker, M. *Catal. Lett.* **2008**, *122*, 210−213.

(10) Bowker, M.; Holroyd, R.; House, M.; Bracey, R.; Bamroongwongdee, C.; Shannon, M.; Carley, A. *Top. Catal.* **2008**, *48*, 158−165.

(11) Routray, K.; Zhou, W.; Kiely, C. J.; Grunert, W.; Wachs, I. E. *J. Catal.* **2010**, *275*, 84−98.

(12) Routray, K.; Wachs, I. E. *Prepr.−Am. Chem. Soc., Div. Pet. Chem.* **2007**, *52*, 25−29.

(13) Glisenti, A.; Favero, G.; Granozzi, G. *J. Chem. Soc., Faraday Trans.* **1998**, *94*, 173.

(14) House, M. P.; Carley, A. F.; Echeverria-Valda, R.; Bowker, M. *J. Phys. Chem. C* **2008**, *112*, 4333−4341.

(15) Tian, H. J.; Roberts, C. A.; Wachs, I. E. *J. Phys. Chem. C* **2010**, *114*, 14110−14120.

(16) Wang, L.; Ma, T.; Sheng, W.; Guo, X.; Ding, W.; Chen, Y. *Chin. J. Catal.* **2009**, *30*, 711−713.

(17) Jin, G.; Weng, W.; Lin, Z.; Dummer, N. F.; Taylor, S. H.; Kiely, C. J.; Bartley, J. K.; Hutchings, G. J. *J. Catal.* **2012**, *296*, 55−64.

(18) Ivanov, K.; Dimitrov, D.; Boyanov, B. *Chem. Eng. J.* **2009**, *154*, 189−195.

(19) Wilson, J. H.; Hill, C. G.; Dumesic, J. A. *J. Mol. Catal.* **1990**, *61*, 333−352.

(20) Beale, A. M.; Jacques, S. D. M.; Sacaliuc-Parvalescu, E.; O'Brien, M. G.; Barnes, P.; Weckhuysen, B. M. *Appl. Catal., A* **2009**, *363*, 143−152.

(21) Uhlrich, J. J.; Sainio, J.; Lei, Y.; Edwards, D.; Davies, R.; Bowker, M.; Shaikhutdinov, S.; Freund, H. J. *Surf. Sci.* **2011**, *605*, 1550−1555.

(22) Al Shihry, S. S.; Halawy, S. A. *J. Mol. Catal A: Chem.* **1996**, *113*, 479−487.

(23) Miao, Y.; Lu, G.; Liu, X.; Guo, Y.; Wang, Y.; Guo, Y. *J. Ind. Eng. Chem.* **2010**, *16*, 45−50.

(24) Briand, L. E.; Hirt, A. M.; Wachs, I. E. *J. Catal.* **2001**, *202*, 268−278.

(25) Davies, R.; Edwards, D.; Gräfe, J.; Gilbert, L.; Davies, P.; Hutchings, G.; Bowker, M. *Surf. Sci.* **2011**, *605*, 1754−1762.

(26) Seyedmonir, S. R.; Abdo, S.; Howe, R. F. *J. Phys. Chem.* **1982**, *86*, 1233.

(27) Belhekar, A. A.; Ayyappan, S.; Ramaswamy, A. V. *J. Chem. Technol. Biotechnol.* **1994**, *59*, 395.

(28) Ressler, T.; Timpe, O.; Neisius, T.; Find, J.; Mestl, G.; Dieterle, M.; Schlogl, R. *J. Catal.* **2000**, *191*, 75−85.

(29) Massa, M.; Haggblad, R.; Hansen, S.; Andersson, A. *Appl. Catal., A* **2011**, *408*, 63−72.

(30) Radhakrishnan, R.; Reed, C.; Oyama, S. T.; Seman, M.; Kondo, J. N.; Domen, K.; Ohminami, Y.; Asakura, K. *J. Phys. Chem. B* **2001**, *105*, 8519−8530.

(31) Ravel, B.; Newville, M. *J. Synchrotron Radiat.* **2005**, *12*, 537−541.

(32) Bowker, M.; Brookes, C.; Carley, A. F.; House, M. P.; Kosif, M.; Sankar, G.; Wawata, I.; Wells, P. P.; Yasenava, I. *Phys. Chem. Chem. Phys.* **2013**, *15*, 12056−12067.

(33) Huang, Y.; Cong, L. Y.; Yu, J.; Eloy, P.; Ruiz, P. *J. Mol. Catal A: Chem.* **2009**, *302*, 48−53.

(34) Newville, M. *J. Synchrotron Radiat.* **2001**, *8*, 322−324.